Correlation between the surface characteristics of carbon supports and their electrochemical stability and performance in fuel cell cathodes

Ignacio Jimenez-Morales, Alvaro Reyes-Carmona, Marc Dupont, Sara Cavaliere, Marlene Rodlert, Flavio Mornaghini, Mikkel J Larsen, Madeleine Odgaard, Jerzy Zajac, Deborah J Jones, et al.

Received: 4 December 2020 | Revised: 12 February 2021 | Accepted: 25 February 2021

DOI: 10.1002/cey2.109

RESEARCH ARTICLE

CARBON ENERGY WILEY

Correlation between the surface characteristics of carbon supports and their electrochemical stability and performance in fuel cell cathodes

Ignacio Jiménez-Morales[1] | **Alvaro Reyes-Carmona**[1] | **Marc Dupont**[1] | **Sara Cavaliere**[1,2] | **Marlene Rodlert**[3] | **Flavio Mornaghini**[3] | **Mikkel J. Larsen**[4] | **Madeleine Odgaard**[4] | **Jerzy Zajac**[1] | **Deborah J. Jones**[1] | **Jacques Rozière**[1]

[1]ICGM Université de Montpellier, CNRS, ENSCM, Montpellier, France

[2]Institut Universitaire de France (IUF), Paris, France

[3]Imerys Graphite and Carbon, Bodio, Switzerland

[4]IRD Fuel Cells A/S, Odense SØ, Denmark

Correspondence
Sara Cavaliere, ICGM Université de Montpellier, CNRS, ENSCM, Place Eugène Bataillon, 34095 Montpellier Cedex 5, France.
Email: sara.cavaliere@umontpellier.fr

Funding information
Institut Universitaire de France, Grant/Award Number: Sara Cavaliere; FP7 Joint Technology Initiatives, Grant/Award Number: 303466 IMMEDIATE

Abstract

In this paper, an extensive characterisation of a range of carbon blacks (CB) with similar surface area but different surface chemistry is carried out by flow calorimetry, Raman spectroscopy, dynamic water vapour sorption, instrumental gas analysis, nitrogen adsorption/desorption and high potential chronoamperometry. Using these carbon materials as supports, Pt/CB electrocatalysts are prepared by microwave-assisted polyol-mediated synthesis in gram scale. Structural, morphological and electrochemical properties of the prepared electrocatalysts are evaluated by X-ray diffraction, transmission electron microscopy, rotating disc electrode and in situ fuel cell characterisation of the corresponding membrane–electrode assemblies. The obtained results allow to establish a relationship between surface chemistry and electrochemical properties useful for the design of Pt/C catalyst layers with high performance and stability.

KEYWORDS
carbon black, electrocatalyst support, fuel cell cathodes, surface properties

1 | INTRODUCTION

Cathodes of proton-exchange membrane fuel cells (PEMFC), where the oxygen reduction reaction (ORR) takes place, face many challenges to meet activity, durability and cost requirements: the reduction of noble metal loading while keeping high electroactivity,[1,2] the mitigation of catalyst and support degradation to enhance the lifetime of the devices[3,4] and the improvement in water management and mass transport to enhance their performance at high current density.[5,6]

Carbon blacks (CB) are low-cost supports conventionally used in PEMFC cathodes. These materials, produced by pyrolysis or incomplete combustion of hydrocarbons, present a turbostratic structure in which the graphene layers are stacked into randomly oriented crystallites[7] and possess high electrical conductivity, porosity and surface area.[3] In start–stop conditions of a

fuel cell, fuel starvation may occur and the local potential of the cathode increases beyond the operation potential, carbon experiences electrochemical corrosion, thermodynamically possible in the presence of water above 0.207 V/RHE, according to the following reaction:

$$C + 2H_2O \rightarrow CO_2 + 4H^+ + 4e^- \quad E^0 = 0.207\,V. \quad (1)$$

Carbon can also be oxidised to carbon monoxide (CO) (2) and further to CO_2 in the presence of water (3)[8]:

$$C + 2H_2O \rightarrow CO + 2H^+ + 2e^- \quad E^0 = 0.518\,V, \quad (2)$$

$$CO + H_2O \rightarrow CO_2 + 2H^+ + 2e^- \quad E^0 = -0.103\,V. \quad (3)$$

On the one hand, this support degradation can lead to the detachment of the anchored Pt nanoparticles and their agglomeration into large clusters, and therefore to their inactivation with the interruption of the triple-phase boundary, loss of electroactive surface area and decrease of the fuel cell performance.[9,10] On the other hand, carbon corrosion can increase the resistance of gas mass transfer, by modifying the properties of the carbon surface (e.g., reducing its hydrophobicity)[11] and breaking down the contact in between primary carbon agglomerates, which reduces the tortuosity of the catalyst layer.[12] Furthermore, the intermediate products of oxidation (e.g., CO; reaction 2) may adsorb on the surface of metal catalyst particles and poison the catalytic sites with a subsequent loss of ORR activity.

Several approaches have been implemented to enhance the corrosion resistance of carbon-based supports including the use of more graphitic carbons[6,13,14] and their coverage or replacement with stable transition metal oxides or carbides.[15–19] The modification of carbon surface properties is another strategy that can also affect mass transfer and water management at high load. The surface of CB generally presents dangling oxygen groups (e.g., hydroxyl, carbonyl and carboxyl groups)[7] that play a role in the dispersion and stability of supported metal nanocatalysts. Modification of the hydrophilic/hydrophobic properties of CB, for instance, by oxidation[20,21] or doping with heteroatoms such as nitrogen[22] or fluorine,[23] was also demonstrated to improve durability and gas transport properties. The surface functionalisation of carbon supports has been demonstrated to affect the ionomer coverage in the catalyst layer as well as its performance and durability in the fuel cell.[24] Therefore, an increasing interest and need is emerging to correlate surface and structure properties of carbon supports with the performance and stability to corrosion of the corresponding PEMFC cathodes.[6,8]

In this study, carbons with a similar surface area but different surface chemistries were used as supports for the deposition of Pt nanoparticles synthesised by the microwave-assisted polyol-mediated method.[25–27] Morphological, structural, textural and surface chemical properties of the carbon support and the corresponding electrocatalysts were investigated. Electrochemical characterisation was performed on the catalysed CB in a rotating disc electrode (RDE) as well as in a single fuel cell, highlighting the correlation between the surface characteristics of the different supports and the activity and durability of the corresponding cathodes. These outcomes contribute to understanding the role of electrocatalyst supports in the catalyst layer structure of PEMFC.

2 | EXPERIMENTAL SECTION

2.1 | Preparation of carbon supports

Six experimental carbons resulting from different production processes and posttreatments were developed by Imerys Graphite & Carbon Switzerland Ltd. The different treatments led to carbons with a nominally similar surface area (S_{BET}) of $400 \pm 50\,m^2 \cdot g^{-1}$ but with different proportions of micropores and mesopores and different surface chemistry characteristics. The carbons were labelled CB1, CB2, CB3, CB4, CB5 and CB6. These carbons were used as support materials for platinum nanoparticles, to give a series of Pt/CB catalysts with a nominal Pt loading of 60 wt%.

2.2 | Preparation of Pt/C catalysts by a microwave-assisted polyol-mediated procedure

For 1-g scale preparation, 2.457 g of hexachloroplatinic acid (99.9 wt%; Alfa Aesar) was dissolved in 2 L of ethylene glycol (EG; 99.8 wt%; Sigma-Aldrich) and saturated with N_2 for 15 min. Then, the pH was adjusted to 11.4 using 1 M NaOH solution in EG (98 wt%; Sigma-Aldrich). The resulting solution was flowed steadily at a rate of $12.5\,mL \cdot min^{-1}$ by means of a peristaltic pump (Watson–Marlow 520DuN IPt/CB66/NEMA 4X) and subjected to 160 W for 4 min in the microwave reactor (MiniFlow 220SS Sairem). The solution was then collected and cooled to prevent any further reaction.[25,27,28] The resulting Pt nanoparticle suspension was acidified to a pH value of 4 by the addition of 1.0 M EG solution of sulphuric acid (H_2SO_4, 96 wt%; Carlo Erba), and then the carbon support (615 mg) was added. The choice of pH value of 4 was based on the results of zeta potential measurements (Figure S1), where the pH at which the charges are opposite and highest is expected to favour nanoparticle (NP)–support interaction. The suspension was ultrasonicated (VWR Ultrasonic Cleaner) for 30 min and stirred for 48 h to allow the Pt nanoparticles to adsorb on the carbon surface. The respective Pt/C samples were then separated by filtration, washed with milli-Q water, ethanol/water mixture and water and dried at 80°C in air

for 24 h. All samples were subjected to a thermal posttreatment at 160°C for 1 h to remove any traces of EG from the Pt surface.[19] To prepare larger amounts of Pt/CB samples (up to 10 g), the microwave-assisted polyol-mediated synthesis was adapted to a continuous flow system.

The Pt/C catalysts are denoted as Pt/CB1, Pt/CB2, Pt/CB3, Pt/CB4, Pt/CB5 and Pt/CB6, corresponding to the use of CB1, CB2, CB3, CB4, CB5 and CB6, respectively, as carbon support. HiSPEC® 9100 (56.81 wt% Pt; Johnson Matthey) was used as a reference catalyst.

2.3 | Carbon support characterisation

2.3.1 | Surface area and pore size distribution

The apparent specific surface area (S_{BET}) of selected catalyst samples was determined by N_2 physisorption measurements at −196°C. The samples were evacuated at 120°C for 12 h before the measurements. Adsorption isotherms were then obtained by the use of a Micromeritics ASAP 2010M instrument. The S_{BET} value was calculated on the basis of the Brunauer–Emmett–Teller (BET) model adapted to describe micropore-containing solids as a rational approximation and by taking 0.162 nm^2 as a cross-sectional area for one adsorbed N_2 molecule. The pore size distribution was calculated from the adsorption branch of the adsorption–desorption isotherms by the Barrett–Joyner–Halenda (BJH) formula, and the microporosity was determined using the *t* plot method. Mercury intrusion porosimetry measurements were made using an AutoPore IV 9500 Micromeritics instrument.

2.3.2 | Raman spectroscopy

Raman spectra of the carbon samples CB1–CB6 were recorded using a Horiba Jobin Yvon equipped with a blue laser diode ($\lambda = 473$ nm) and a scan surface of 100 μm^2. The ratio between the G- and D-peak intensities, respectively, at ca. 1580 and 1350 cm^{-1}, was used to estimate the in-plane crystallite size (L_a).[29] Analysis of the G-peak position and full width at half maximum (FWHM) also provided information on the degree of crystallinity of the series of carbons.

2.3.3 | Dynamic vapour sorption

Dynamic gravimetric water vapour sorption measurements were performed at 22°C on the carbon samples CB1–CB6 at relative humidities (RH) between 2% and 93% to determine their gravimetric water uptake/loss during adsorption and desorption. Samples were dried at 90°C under vacuum before the adsorption measurement. A high-resolution microbalance (μg) was used to determine weight changes, and the equilibration time was 1 h for each data point.

2.3.4 | Instrumental gas analysis (IGA) of oxygen content

The oxygen content of the carbons was determined with IGA by heating the samples in a graphite crucible at 2000°C and analysing the gases released by gas chromatography.

2.3.5 | Zeta potential measurements

Zeta potential measurements of carbon supports and Pt NPs were carried out to determine the optimal pH conditions to adsorb Pt on carbon surfaces. In a typical procedure, 1 mg of each material was dispersed in 10 mL of MilliQ water and sonicated for at least 10 min. The zeta potential of the resulting suspension was monitored as a function of pH (modified by adding drops of HNO_3 or NaOH solutions; Sigma-Aldrich), ranging from 2 to 8, using a Malvern Zetasizer 3000 device.

2.3.6 | Determination of surface polar sites, hydrophobic and aromatic character

Surface characteristics of the carbon materials were analysed by nondestructive liquid-flow calorimetry using a Mark IV Microscale Flow Microcalorimeter, in which enthalpy changes due to the competitive adsorption of probe molecules from either water or *n*-heptane at 293 K were determined. In each case, a carbon sample was placed in the flow cell, and the cell was evacuated to 0.1 mmHg and wetted with solvent (water or *n*-heptane), which was subsequently percolated through the sample at a rate of 4.2 $mL \cdot h^{-1}$. Once thermal equilibrium was attained (<60 min), the flow of the solvent was exchanged for that of the appropriate solution: 2 $g \cdot L^{-1}$ solution of *n*-butanol in *n*-heptane, 10 $g \cdot L^{-1}$ solution of *n*-butanol in water and 2 $g \cdot L^{-1}$ solution of *n*-dotriacontane in *n*-heptane to quantify the hydrophilic, hydrophobic and aromatic character, respectively.[30,31] The displacement of the solvent by the adsorbing solute molecules alters the thermal equilibrium and induces a thermal effect, which is recorded by the thermistors as a thermal peak, where the area under the peak is proportional to the total

heat evolved. A calibration coil in the cell allowed the correlation between the fixed energy supplied and the integrated value to be established. The enthalpy change measured in a given displacement experiment represents the integral enthalpy of adsorption from solution per unit mass of adsorbent, namely $\Delta_{ads}H_{BW}$ and $\Delta_{ads}H_{BH}$ which are the enthalpies of butanol adsorption from its solutions, respectively, in water and *n*-heptane, whereas $\Delta_{ads}H_{DH}$ is the enthalpy of *n*-dotriacontane adsorption from its solution in *n*-heptane.

2.4 | Pt/carbon catalyst characterisation

2.4.1 | Determination of Pt loading

The amount of Pt deposited on the carbon supports was determined by X-ray fluorescence (XRF). Pt/C samples (30 mg) were ground with 100 mg of boric acid. The Pt/C–H_3BO_3 powder was pressed in a 13-mm die to obtain a pellet with a scanned surface diameter of ca. 12 mm. The same procedure was followed to prepare three standards using 50, 60 and 70 wt% of Pt black (Alfa Aesar) and CB to obtain a calibration line. The XRF analyses were performed with a PANalytical Axios Max spectrometer fitted with an Rh (4 kW) tube and equipped with a LiF200 crystal and Omnian software.

2.4.2 | Determination of Pt particle size

The morphology and distribution of the Pt particles on carbons were analysed by transmission electron microscopy (TEM) using a JEOL 1200 EXII microscope operating at 120 kV and equipped with a CCD camera SIS Olympus Quemesa (11 million pixels). The samples were suspended in ethanol and sonicated before deposition on carbon-coated copper grids. The particle size distribution and mean diameter (number average) of the Pt NPs were obtained by counting and measuring 200 particles using the ImageJ software.

Powder X-ray diffraction (XRD) patterns were recorded at room temperature in Bragg–Brentano configuration using a PANalytical X'pert diffractometer, equipped with a hybrid monochromator, operating with CuK_α radiation ($\lambda = 1.541$ Å), and using a step size of 0.1° 2θ within the 2θ domain from 20° to 80°. The diffraction patterns were analysed by the Fityk program using the Pseudo-Voigt fitting method. The Pt nanocrystallite size was calculated from the Scherrer formula using the Pt(111) diffraction line, measuring the FWHM parameter by a graphical method.

2.5 | Electrochemical characterisation of carbon supports and Pt/C catalysts

A conventional three-electrode cell consisting of a glassy carbon RDE was used to characterise carbon supports and Pt/C catalysts. The cell was equipped with a glassy carbon working electrode of geometric area 0.196 cm^2, a reversible hydrogen electrode (RHE; reference electrode) and a platinum wire (counter electrode). A Pine bipotentiostat model AFCBP1 was used. All the potential values are referred to the RHE, and the current densities are reported as current per geometric electrode area.

For the measurement of carbon support corrosion, inks were prepared by dispersing 10 mg of carbon in 35 μL of milli-Q water, 100 μL of 5 wt% Nafion® solution in alcohols (Sigma-Aldrich) and 1.3 mL of ethanol (Sigma-Aldrich) by ultrasonication (VWR Ultrasonic Cleaner). Also, 8 μL of the resulting suspensions were deposited on the working electrode surface with a micropipette. The carbon supports were submitted to a potentiostatic accelerated stress test (AST) consisting of chronoamperometry measurements in 0.5 M H_2SO_4 at 80°C, with the working electrode potential hold at 1.4 V versus RHE for 2 h.

Catalyst ink for the electrochemical characterisation of the Pt/C samples was prepared by dispersing 5 mg of Pt/C (or the HiSPEC 9100 reference) in 1 mL milli-Q water, 4 mL of 2-propanol (Sigma-Aldrich) and 35 μL of 5 wt% Nafion® solution in alcohols (Sigma-Aldrich). The catalyst inks were sonicated (VWR Ultrasonic Cleaner) for 15 min. Aliquots of 7 μL of the inks were then deposited on the RDE surface with a micropipette and dried in air. The Pt loading in each case was 21.3 $\mu g \cdot cm^{-2}$. Cyclic voltammetry (CV) was performed in N_2-saturated 0.1 M $HClO_4$ at 20°C. The sample surfaces were cleaned by performing 100 voltage cycles between 0.025 and 1.2 V versus RHE at a rate of 500 $mV \cdot s^{-1}$ in N_2-saturated electrolyte, after which the electrochemically active specific surface area (ECSA) of the platinum was determined from voltammograms recorded in the same potential range at a scan rate of 20 $mV \cdot s^{-1}$ in N_2-saturated electrolyte. The hydrogen desorption peaks in the range 0.05–0.4 V versus RHE were used to determine the ECSA after double-layer correction, assuming a monolayer hydrogen adsorption charge of 210 $\mu C \cdot cm^{-2}$ on the Pt surface. The electrocatalytic activity toward the ORR was evaluated from voltammograms recorded using linear sweep voltammetry at 1600 rpm in O_2-saturated 0.1 M $HClO_4$. The potential was varied from 0.01 to 1.2 V versus RHE at a scan rate of 20 $mV \cdot s^{-1}$, and the ORR activity was evaluated at 0.90 and 0.95 V versus RHE. These measurements were later background- and

IR-corrected. Specific activity (i_k) and mass activity ($i_{k,\,mass}$) were obtained by division of I_k by the ECSA and the mass of Pt in the electrode (m_{Pt}), respectively.

Each Pt/C electrocatalyst was subjected to two AST procedures.[32] The first, designed to evaluate the stability of the platinum nanoparticles, involved 10,000 potential cycles between 0.6 and 1.0 V/RHE at room temperature and a scan rate of 500 $mV{\cdot}s^{-1}$. The second AST, which was carried out on a second sampling of each Pt/C material, targeted acceleration of the carbon support corrosion. It consisted of 6000 electrochemical cycles at room temperature and a scan rate of 100 $mV{\cdot}s^{-1}$ between 1.0 and 1.6 V/RHE, where carbon corrosion can be severe. In both ASTs, voltammograms were recorded as described above, before the first measurement (beginning of the test [BoT]), then every 100 cycles and at the end of the test (EoT), to determine the evolution of ECSA, i_k and $i_{k,\,mass}$.

2.6 | Preparation of membrane–electrode assemblies (MEAs) with Pt/CB cathodes and single-cell characterisation

Here, 25-cm^2 MEAs were prepared by catalyst-coated membrane method with 0.1 mg $Pt{\cdot}cm^{-2}$ anode, 0.3 mg $Pt{\cdot}cm^{-2}$ cathode based on Pt/CB, SGL grade 28 BC gas diffusion layers and a 15-μm Fumasep FS-720 membrane. The MEA was incorporated into the fuel cell fixture using fluorinated ethylene propylene gaskets at 10%–15% compression. The prepared MEAs were conditioned at 0.4 $A{\cdot}cm^{-2}$ overnight at 100% RH and 80°C. Polarisation curves were recorded on H_2/air (stoichiometry 1.5/1.8) in dry (40% RH, 1.5 bar absolute pressure, 80°C) and wet (100% RH, 2.5/2.3 bar absolute pressure, 80°C) conditions.

3 | RESULTS AND DISCUSSION

3.1 | Textural properties of CB

The values of the apparent BET surface area of the CB have been collected in Table 1. These results indicate that the apparent specific surface areas lie in the range of 350–450 $m^2{\cdot}g^{-1}$. Analysis of the adsorption branch of the isotherms with the BJH formula and *t* plot calculations provided consistent results for each of the carbons, with the sum of the micropore and mesopore percentage approximating 100% in each case. All the carbon materials exhibit pronounced mesoporosity varying from 70% to 100% of the total BET surface area. The two carbon samples having the highest and lowest surface areas, CB3 the highest and CB6 the lowest, are both essentially devoid of micropores. The proportion of micropores (0%–20%) is low, which is highest for CB5. The total accessible volume was also analysed by mercury porosimetry. The measurements indicated that CB6 possessed a much larger total volume intruded than the other carbon supports, whereas CB5 had the least total accessible volume.

3.2 | Flow calorimetry measurements on CB

The surface hydrophilic–lipophilic balance and the aromatic character of the six catalyst supports were evaluated by means of liquid-flow calorimetry. The principle of the method is based on the competitive adsorption of molecular probes that can interact specifically with different parts of the carbon surface when dissolved in the corresponding solvent, allowing the excess energy of such interactions to be quantified. As this excess energy is considered to be much less sensitive to the

TABLE 1 Apparent surface area and pore size properties of carbon materials analysed by N_2 physisorption and mercury intrusion porosimetry

Carbon support	S_{BET} ($m^2{\cdot}g^{-1}$) (BET)	Micropores (%) (*t* plot)	Mesopores (%) (BJH)	Total volume of open pores ($ml{\cdot}g^{-1}$) (Hg intrusion)
CB1	384	13.5	87	6.1
CB2	385	9.1	93	5.4
CB3	452	1.6	100	5.1
CB4	371	14.5	73	4.3
CB5	379	19.7	76	1.5
CB6	349	7.0	100	8.1

Abbreviations: BET, Brunauer–Emmett–Teller; BJH, Barrett–Joyner–Halenda.

surface energetic heterogeneity than are the absolute energy parameters, the average enthalpy of competitive adsorption measured in a single calorimetric run provides an estimate of the extent of the carbon surface with which the probe molecule interacts preferentially in the presence of a given solvent.

n-Butanol has significant solubility in water, owing to its amphiphilic molecular structure comprising a short alkyl chain having four carbon atoms and one terminal hydroxyl group, and it can interact selectively (more strongly as compared with water molecules) with different nonpolar sites on the carbon surface. The concentration of the butanol solution in water used in the present study ($10\,g{\cdot}L^{-1}$) was previously optimised to be sufficiently concentrated for the adsorbed solute molecules to form a monolayer on the carbon surface.[33] On the contrary, it is sufficiently dilute to preclude any dimerisation of butanol units in the liquid phase. The Van der Waals radius of butanol is 0.558 nm and it can, therefore, penetrate into the meso and the larger micropores. Finally, as the alcohol units enter in competition with water molecules for nonpolar surface sites, the enthalpy of butanol adsorption from aqueous solution per unit mass of the adsorbent is a measure of the hydrophobic surface area accessible to this adsorbate.

The *n*-butanol molecules are bipolar according to the nomenclature introduced by Van Oss et al.[34] and as such, they may interact with a polar surface site by both their (Lewis) acidic and basic functionality. They can thus be used to titrate the acidic and basic sites of powdered carbonaceous samples. To avoid the Van der Waals' contribution to the enthalpy of adsorption, the *n*-butanol titrant is adsorbed from a hydrophobic solvent (*n*-heptane).[30] As the $2\,g{\cdot}L^{-1}$ solution of butanol in *n*-heptane was previously optimised to obtain a monomolecular solute adsorption, the area of hydrophilic surface of the carbon catalysts accessible to this alcohol can be estimated on the basis of the enthalpy of butanol adsorption from *n*-heptane.

Finally, the graphitic character of the catalyst surface can be investigated by determining the preferential adsorption of *n*-dotriacontane, $C_{32}H_{66}$, from a $2\,g{\cdot}L^{-1}$ solution in *n*-heptane. This straight-chain hydrocarbon containing 32 carbon atoms is capable of adsorbing preferentially over the solvent on the graphitic basal planes, being strongly localised on polycondensed aromatic domains. Here, the enthalpy of *n*-dotriacontane adsorption from *n*-heptane per unit mass of carbon is considered as a measure of the surface area of the extended aromatic surface.

The results obtained, summarised in Table 2, indicate that all investigated carbon supports had a predominantly hydrophobic character. The hydrophilic surface domains were a very limited fraction of the total area, thereby giving small enthalpy signals at the limit (or even below, for CB6) of detection. Their surface hydrophilic–hydrophobic ratios were generally below 10%, which is similar to those obtained with very hydrophobic activated carbons.[33] Two samples emerged concerning their several times higher hydrophilic character: CB3 and particularly CB5. CB4 had the most hydrophobic and CB5 the most hydrophilic surface. The porosity of the samples can also have an important effect on the surface hydrophilic–lipophilic balance, as inferred from the competitive adsorption of *n*-butanol from water or *n*-heptane.

Furthermore, most of the carbon surface had an aromatic character, as indicated by high $\Delta_{ads}H_{DH}$ values. As a result, long *n*-dotriacontane molecules were capable of displacing the pre-adsorbed solvent (*n*-heptane) units and were retained over extended aromatic domains in an orientation parallel to the surface. The aromatic surface area of the carbon samples increased in the following order: $CB5 \ll CB4 < CB2 < CB1 < CB6 < CB3$, where the most hydrophilic sample (CB5) is also that with the lowest aromatic surface. The reason may be that the dispersion of numerous polar sites over the carbon surface hinders the hydrophobic attachment of *n*-dotriacontane molecules to the underlying aromatic domains. These results provide a new perspective of the nature of the carbon supports and the insights are expected to allow a better understanding of

TABLE 2 Hydrophobic, hydrophilic and aromatic character of carbon supports evaluated by flow calorimetry

Carbon support	Hydrophobic character $\Delta_{ads}H_{BW}$ ($J{\cdot}g^{-1}$)	Hydrophilic character $\Delta_{ads}H_{BH}$ ($J{\cdot}g^{-1}$)	Hydrophilic–hydrophobic ratio $\Delta_{ads}H_{BH}/\Delta_{ads}H_{BW}{\cdot}100\%$	Aromatic character $\Delta_{ads}H_{DH}$ ($J{\cdot}g^{-1}$)
CB1	42.2	2.4	5.7	56.1
CB2	45.2	2.9	6.4	49.7
CB3	48.6	6.0	12.3	74.3
CB4	54.8	1.6	2.9	47.2
CB5	40.4	9.9	24.5	14.3
CB6	38.6	-	-	62.7

the relationship between surface, electrochemical and durability characteristics. Complementary experimental techniques were used to confirm the results obtained.

3.3 | Water vapour adsorption and IGA

Dynamic water vapour sorption analysis was performed on the six carbon supports recording the change in their weight in an environment of controlled RH. The results obtained at low (40%) and high RH (80%) (Table 3) showed the same trend and indicated that, to a first approximation, CB1–CB4 carbons have a similar weight increase; however, CB6 took up notably less water and CB5 significantly more. These trends are fully consistent not only with the hydrophilic character assessed by flow microcalorimetry, but also with the oxygen content determined by IGA analysis, with CB5 having the highest oxygen content and CB6 the lowest oxygen content (Table 3). This good agreement further infers that the polar sites detected by flow calorimetry mainly contain oxygen, rather than nitrogen or other polar elements.

3.4 | Raman spectroscopy

Raman spectroscopy was performed to assess the degree of graphitisation of the different CB. Raman spectra of all samples presented two bands at 1580 and 1350 cm^{-1}, respectively, the G band (from graphite) and the D band (D for defect or disorder).[35] The intensity of the latter is proportional to the amount of disorder (crystallite boundary) in the sample, and the ratio between the intensities of the first-order graphite G band and the disorder-induced D band (I_G/I_D) provides a parameter that can be used to quantify disorder and correlate with

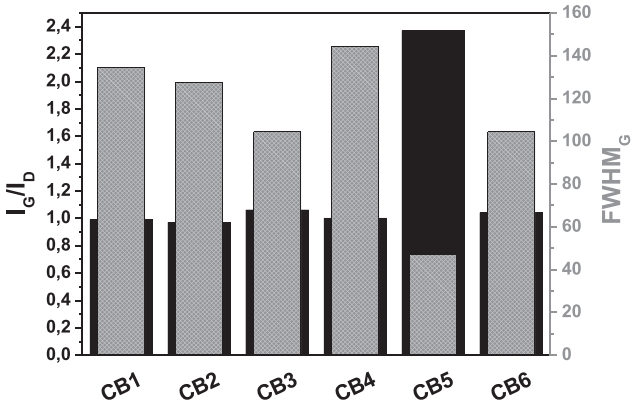

FIGURE 1 Full width at half maximum (FWHM) of the G-band (FWHM$_G$), and I_G/I_D band ratio derived from Raman spectra of carbon samples CB1–CB6

crystallite size, L_a (L_a (nm) = 4.4 I_G/I_D).[36] In the present work, the intensity ratio (I_G/I_D) (Figure 1) is essentially identical for carbon samples CB1–CB4 and CB6, whereas for CB5, it was a factor 2–3 times higher, showing significantly greater crystallite size. The width of the G-band (FWHM$_G$, see Figure 1) also provides information on the crystallite size (FWHM (G) = 14 + 430/L_a).[37] In the present case, the FWHM appears to be more sensitive to the crystallite size than the I_D/I_G ratio. The narrower line width for CB5 corroborates the above conclusion of a greater crystallite size (ca. 11 vs. 4 nm of the other samples). Furthermore, from FWHM values, the following crystallite size order for all the carbon samples may be inferred as follows: CB5 ≫ CB3 ≈ CB6 > CB2 > CB1 > CB4. This order is the inverse as that given by the empirical relation [($\Delta_{ads}H_{BW}/\Delta_{ads}H_{BH}$)($\Delta_{ads}H_{DH}$)], that is, the product of the hydrophobic/hydrophilic ratio and the aromatic character from flow microcalorimetry.

TABLE 3 Water uptake and oxygen content of carbon supports, and their corrosion charge and mass loss at 1.4 V/RHE

Carbon support	Mass increase at 40% RH (%)[a]	Mass increase at 80% RH (%)[a]	Oxygen content (%)[b]	Corrosion charge ($C \cdot mg^{-1}$)	Carbon mass loss (%)
CB1	0.19	4.98	0.21	3.4	10.6
CB2	0.28	4.89	0.19	3.7	11.4
CB3	0.19	6.04	0.17	5.5	16.9
CB4	0.38	8.08	0.20	4.4	13.5
CB5	1.66	10.57	0.57	5.3	16.5
CB6	0.05	2.8	0.05	3.9	12.2

Abbreviations: IGA, instrumental gas analysis; RH, relative humidity; RHE, reversible hydrogen electrode.

[a]From dynamic water vapour sorption analysis.

[b]From IGA.

3.5 | Carbon corrosion at high potential

Electrochemical corrosion of carbon is thermodynamically possible, though kinetically slow, in the conditions of normal operation of a PEMFC according to Equation (1). Uncontrolled excursions to high potential such as on cell reversal induced by fuel starvation on start/stop, as well as increased cell temperature, exacerbate carbon oxidation, with consequent modification of pore size characteristics and hydrophobic/hydrophilic balance. These effects can lead to loss of Pt nanoparticles from the carbon surface and their electrical isolation/inactivation and aggregation, with a concomitant decrease in the ECSA and catalyst activity. In the present work, chronoamperometry was performed at 1.4 V versus RHE and at high temperature (80°C), and carbon degradation was estimated from the integrated corrosion currents (Table 3), which result from the oxidation of carbon to CO_2.[15,25]

The highest corrosion currents and carbon mass losses were observed for CB3 and CB5. These two types of carbon had the highest number of polar sites and the highest hydrophilic/hydrophobic ratio, as determined by flow calorimetry (Table 2). At this point, it is possible to infer that the presence of polar sites and hydrophilic regions increases the propensity to oxidation at a high potential. It can be noticed that CB5 displayed the lowest FWHM of the Raman G band of all the samples, which, according to a recent paper,[6] should result in the highest resistance to corrosion. The lowest electrochemical stability observed for CB5 suggests that hydrophilic character and polarity prevail over graphitisation effects evidenced by Raman spectroscopy. Among the other investigated samples, CB1, which had one of the highest values of aromatic character, presented the lowest corrosion charge.

3.6 | Structural and morphological characterisation of Pt/CB catalysts

XRF results indicated a Pt loading of ca. 60 wt% for all catalysts. XRD diffractograms of the Pt/C materials (Figure S2) display diffraction lines at $2\theta = 39.7°$, 46.2° and 67.4°, characteristic of platinum (JCPDS 004-0802). The average diameter of the Pt crystallites, estimated from the Scherrer equation to the Pt(111) peak, was 3.0–3.5 nm.

A representative example of a TEM micrograph and particle size distribution of a Pt/C electrocatalyst is provided in Figure 2, while those for the other samples are reported in the Supporting Information (Figure S3). Pt particles are uniformly dispersed without aggregation on all the carbon supports. The average particle size is in the range of 2.9–3.2 nm, in agreement with the Pt domain size estimated from XRD patterns.

3.7 | Ex situ electrochemical characterisation of Pt/CB catalysts

Structural and electrochemical characterisation of Pt/CB samples showed that the electrocatalyst based on CB5 was significantly less stable and less active than those prepared with the other carbon supports. This behaviour can be explained in light of the results described above: CB5 presented the highest oxygen content as well as the highest hydrophilic/hydrophobic balance of all the series of supports. The significant hydrophilic character may explain the degradation of Pt/CB5, related to the poor resistance of the support to corrosion (see Equation 1). The presence of a significant amount of oxygen on carbon may impede the attachment of Pt to the support surface. Whereas the introduction of oxygen surface groups may improve metal–support interaction

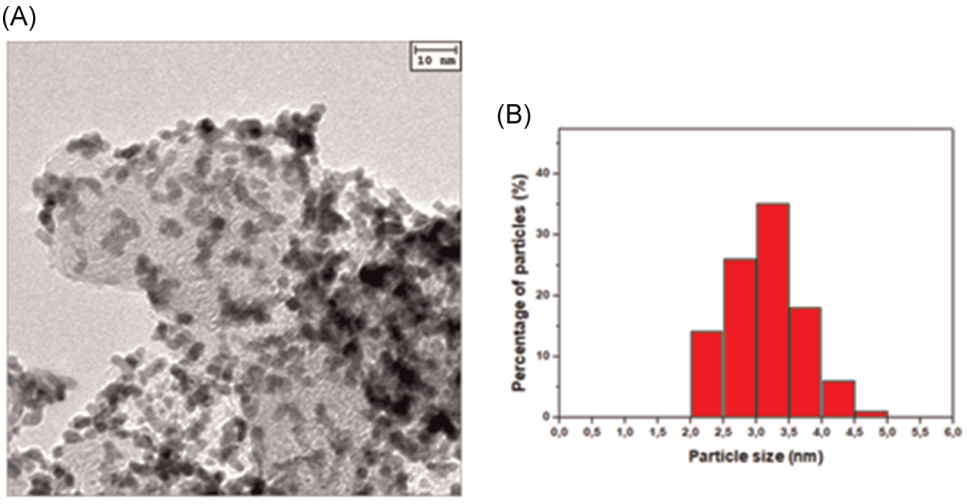

FIGURE 2 (A) Transmission electron micrograph of Pt/CB6 and (B) corresponding histogram of Pt particle size distribution

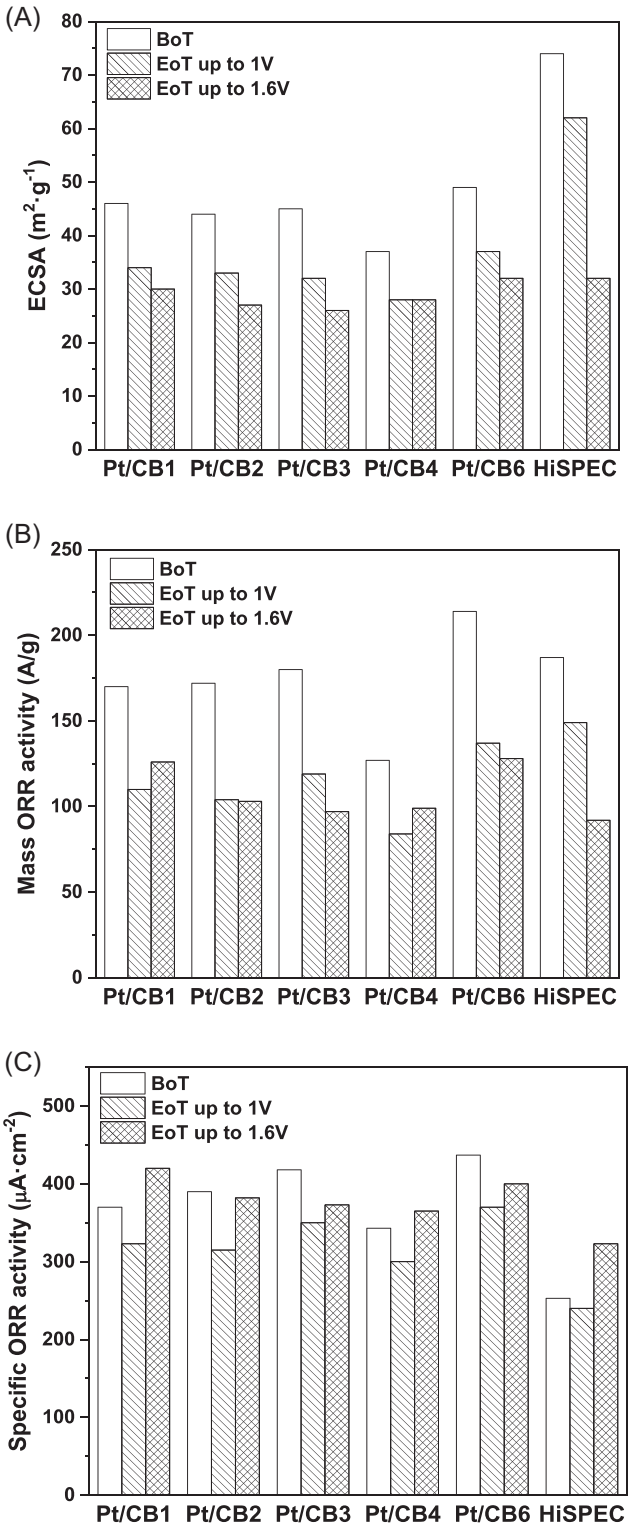

FIGURE 3 Evolution of (A) electrochemical active surface area (ECSA), (B) oxygen reduction reaction (ORR) mass and (C) specific activity at 0.9 V/RHE before and after the accelerated stress test (beginning [BoT] and end of the test [EoT]) indicated in the figure for the prepared catalysts and the reference HiSPEC 9100

for Pt/C samples prepared by impregnation/reduction in an aqueous medium,[38,39] in nonaqueous synthesis routes (including the polyol method), this interaction may be weakened by the reduction of basic sites, which play a primary role in metal adsorption.[40,41] For these reasons, the sample Pt/CB5 was not retained for further characterisation.

Electrochemical characterisation of the other Pt/CB catalysts was carried out and compared with the reference HiSPEC 9100. Cyclic voltammograms recorded in nitrogen-saturated $HClO_4$ (Figure S4a) were consistent with the underpotential adsorption/desorption of hydrogen (H_{upd}) in the potential region $E < 0.4$ V/RHE and Pt oxide formation and reduction in the potential region $E > 0.6$ V/RHE. Electrochemical specific surface area calculated from H_{upd} peaks was significantly lower for Pt/CB materials (around 43 $m^2 \cdot g_{Pt}^{-1}$) than the reference HiSPEC 9100 (74 $m^2 \cdot g_{Pt}^{-1}$) (Table S1). This may be attributed to the smaller metal particle size in the reference catalyst (2.6 nm)[16] as well to the higher surface area of the support, leading to greater accessibility of the electrocatalytic sites considering the high Pt loading (ca. 60 wt%). Linear sweep voltammograms were recorded in O_2-saturated electrolyte (Figure S4b). ORR mass and specific activities were calculated at 0.9 V/RHE (ORR $MA_{0.90\,V/RHE}$ and ORR $SA_{0.90\,V/RHE}$, respectively).

The results, collected in Table S1, show that all the Pt/C catalysts provide a mass activity in the range 170 ± 40 A·g_{Pt}^{-1}, which is similar to that of the reference catalyst, 187 A·g_{Pt}^{-1}, with Pt/CB6 displaying the highest mass activity of 214 A·g_{Pt}^{-1} and Pt/CB4 the lowest, 127 A·g_{Pt}^{-1}. The ORR specific activity for all the samples is significantly higher than that of HiSPEC 9100 (390 ± 50 vs. 253 $\mu A \cdot cm_{Pt}^{-2}$).

Electrochemical accelerated stress testing was carried out on the Pt/CB samples by voltage cycling between 0.6 and 1.0 V versus RHE to promote oxidation/dissolution of platinum. The evolution of ECSA and ORR electrocatalytical activity was evaluated at BoT and EoT, respectively. The results show that the loss of electrochemical surface area and mass activity of the prepared Pt/CB catalysts after voltage cycling was higher than that for HiSPEC 9100 (ECSA loss ca. 25% vs. 16% and MA loss ca. 35% vs. 20%) (Figure 3).

To specifically accelerate corrosion of the carbon support, AST cycling at a higher voltage (between 1.0 and 1.6 V vs. RHE) was carried out (Figure 3). The ECSA drop was significantly lower for all the Pt/CB (ca. −35%) as compared with the HiSPEC 9100 reference (−57%). The mass activity was reduced by around 36% for the Pt/CB catalysts, whereas it was halved for the commercial reference. Among the prepared catalysts, Pt/CB4 exhibited the highest stability at high potential excursion, whereas Pt/CB6 and Pt/CB3 were the most unstable, with a higher loss of ECSA and activity.

TEM analysis before and after the voltage cycling AST showed that the average particle size increases after voltage cycling of 0.6–1.0 V from ca. 3 nm to an average of 4.5 nm and after voltage cycling between 1.0 and 1.6 V to an average diameter of 4.9 nm (Table S2). After the cycling test to 1 V/RHE (Figure S5a1,b1,c1), HiSPEC 9100 reference electrocatalyst shows a homogeneous distribution, as well as the lowest increase of platinum nanoparticles size, compared with all platinum-based carbon supports. Pt/CB4 shows the most homogeneous distribution after the high-voltage AST (Figure S5a2,b2,c2), with a slight increase of platinum nanoparticle size, whereas Pt/CB3 and the reference electrocatalyst exhibit a less uniform distribution and the highest agglomeration of platinum nanoparticles, which is in agreement with the electrochemical characterisation.

These results suggest a possible effect of the hydrophobic character of the support on the stability to corrosion, with CB4 being the most hydrophobic carbon, CB6 the least hydrophobic and CB3 the most hydrophilic (Table 2). According to Equation (1), water repulsion from the catalyst surface would limit corrosion. Oxidation of carbon to CO_2 involves the agglomeration of platinum nanoparticles and even their detachment, therefore leading to lower ECSA and electrochemical activity. This may explain the higher degradation of the hydrophilic sample Pt/CB3 as well as the stability of the more hydrophobic Pt/CB4.

3.8 | In situ electrochemical characterisation of Pt/CB catalysts

MEAs with the Pt/CB electrocatalysts CB1–CB4 and CB6 at the cathode side were characterised in H_2/air single fuel cells. To investigate the role of carbon surface properties and the interaction with water, two conditions of hydration were investigated, 100% and 40% RH. The corresponding polarisation curves are depicted in Figures 4 and 5.

In the polarisation curve recorded under fully hydrated conditions (Figure 4), the open-circuit voltage (OCV) was around 0.98 V for all the MEAs. At low current densities, the behaviour was similar for all the MEAs, except for that with Pt/CB3 at the cathode, which exhibited a slightly lower performance. In the Ohmic region, the slope was similar for all the polarisation curves. Significant differences were observed at the current density above 0.5 A·cm^{-2}, with higher cell voltage for the MEAs with cathodes comprising Pt/CB4, Pt/CB2 and Pt/CB3, which reached maximum power density of 0.75 and 0.77 W cm^{-2} at 1.4 A·cm^{-2} for Pt/CB2 and Pt/CB4, respectively. All the other assemblies demonstrated a high drop in performance ascribed to mass transport resistance. In particular, the MEAs with CB6 at the cathode

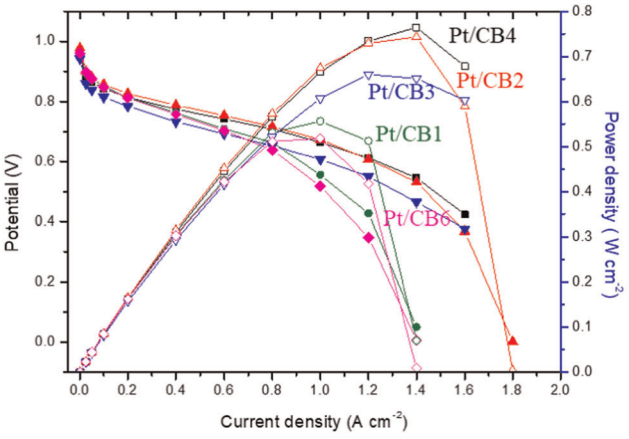

FIGURE 4 Polarisation curves recorded under hydrogen/air at 80°C, 100% RH, using the Pt/CB indicated in the figure in the cathode layer. CB, carbon black; RH, relative humidity

could not reach a current density higher than 1.4 A·cm^{-2}. This result may be correlated with the surface properties of the used CB (Table 2): CB4, CB3 and CB2, presenting the highest hydrophobic character, did not suffer from flooding and corresponding mass transport overpotential, as they were able to remove the water already present in the system (100% RH) and that progressively produced at the cathode side when increasing current density.

A similar trend is evident in Figure 5, where H_2/air polarisation curves of the CB-based MEAs in drier conditions (40% RH) are depicted. The OCV was still around 0.98 V for all MEAs. At high current density, the Pt/CB4-, Pt/CB3- and Pt/CB2-based MEAs again provide higher cell voltage. In these conditions, the maximum power density achieved by them was 0.5 W·cm^{-2} at 1 A·cm^{-2}. These cathodes prepared using the most hydrophobic carbons appear to allow mass transfer at the active sites

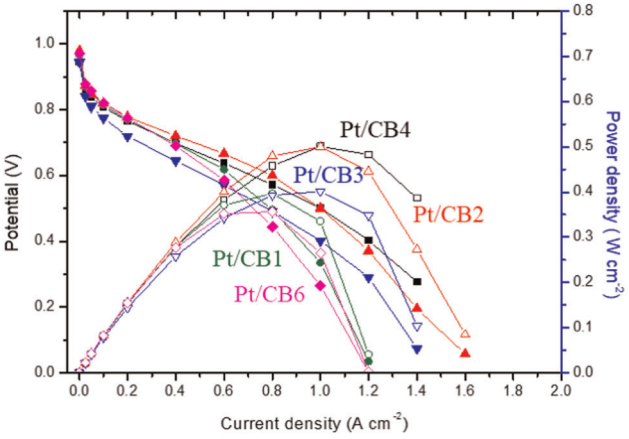

FIGURE 5 Polarisation curves recorded under hydrogen/air at 80°C, 40% RH, using the Pt/CB indicated in the figure in the cathode layer. CB, carbon black; RH, relative humidity

by avoiding blocking of the cathode porosity with the water produced at high current density. In agreement with this observation, the MEA comprising the least hydrophobic carbon black (CB6) at the cathode side gave the lowest performance with a significant drop in cell voltage at high current density.

These results confirmed those obtained in RDE and clearly linked the surface properties of the carbon support in terms of hydrophilicity/hydrophobicity as to *I–V* characteristics of corresponding fuel cell MEAs. The CB with the greatest hydrophobic character and lowest hydrophilic/hydrophobic ratio, CB4, when loaded with Pt particles, led to higher performance in fuel cell MEAs as well as higher stability to corrosion. This suggests that the hydrophobic character of the carbon support not only affects the resistance to corrosion (a reaction needing water to occur), but also the more complex phenomena taking place at the triple-phase boundary regions in fuel cells. In particular, this study evidenced the role of mass transfer closely related with the presence of water in the operation conditions (high RH and high current density). The role of surface chemistry of carbon supports in electron and proton transfer and surface reaction mechanisms still remains a challenging open question to address.

4 | CONCLUSION

CB with a similar surface area and different surface chemistry were characterised with a range of techniques including flow calorimetry to quantify their hydrophilic, hydrophobic and aromatic character. These surface properties play a role in the electrochemical and durability characteristics of the corresponding electrocatalysts and catalyst layers. Among the prepared Pt/CB electrocatalysts, the improved ORR activity, durability and mass transfer observed for samples based on CB4 and CB2 can be ascribed to their higher hydrophobic character. Water removal from such surfaces may be responsible for their lower carbon corrosion as well as lower mass transfer limitation at high current densities, with a beneficial influence on performance, durability and water management.

ACKNOWLEDGEMENTS

Sara Cavaliere acknowledges Institut Universitaire de France (IUF) for financial support. The research leading to these results has received funding from the European Union's Seventh Framework Programme for the Fuel Cells and Hydrogen Joint Undertaking under Grant Agreement 303466 IMMEDIATE.

ORCID

Sara Cavaliere http://orcid.org/0000-0003-0939-108X

REFERENCES

1. Ercolano G, Cavaliere S, Rozière J, Jones DJ. Recent developments in electrocatalyst design thrifting noble metals in fuel cells. *Curr Opin Electrochem*. 2018;9:271-277.
2. Jaouen F, Jones D, Coutard N, Artero V, Strasser P, Kucernak A. Toward platinum group metal-free catalysts for hydrogen/air proton-exchange membrane fuel cells. *Johnson Matthey Technol Rev*. 2018;62(2):231-255.
3. Du L, Shao Y, Sun J, Yin G, Liu J, Wang Y. Advanced catalyst supports for PEM fuel cell cathodes. *Nano Energy*. 2016;29:314-322.
4. Borup R, Meyers J, Pivovar B, et al. Scientific aspects of polymer electrolyte fuel cell durability and degradation. *Chem Rev*. 2007;107(10):3904-3951.
5. Shahgaldi S, Hamelin J. Improved carbon nanostructures as a novel catalyst support in the cathode side of PEMFC: a critical review. *Carbon*. 2015;94:705-728.
6. Tamaki T, Wang H, Oka N, Honma I, Yoon SH, Yamaguchi T. Correlation between the carbon structures and their tolerance to carbon corrosion as catalyst supports for polymer electrolyte fuel cells. *Int J Hydrog Energy*. 2018;43(12):6406-6412.
7. Boehm HP. Some aspects of the surface chemistry of carbon blacks and other carbons. *Carbon*. 1994;32(5):759-769.
8. Shin H-S, Kwon O-J, Oh BS. Correlation between performance of polymer electrolyte membrane fuel cell and degradation of the carbon support in the membrane electrode assembly using image processing method. *Int J Hydrog Energy*. 2018;43(45):20921-20930.
9. Meier JC, Galeano C, Katsounaros I, et al. Degradation mechanisms of Pt/C fuel cell catalysts under simulated start-stop conditions. *ACS Catal*. 2012;2(5):832-843.
10. Yu Y, Li H, Wang H, Yuan XZ, Wang G, Pan M. A review on performance degradation of proton exchange membrane fuel cells during startup and shutdown processes: causes, consequences, and mitigation strategies. *J Power Sources*. 2012;205:10-23.
11. Yang Z, Chen M, Xia M, Wang M, Wang X. An effective and durable interface structure design for oxygen reduction and methanol oxidation electrocatalyst. *Appl Surf Sci*. 2019;487:655-663.
12. Ghosh S, Ohashi H, Tabata H, Hashimasa Y, Yamaguchi T. In-plane and through-plane non-uniform carbon corrosion of polymer electrolyte fuel cell cathode catalyst layer during extended potential cycles. *J Power Sources*. 2017;362:291-298.
13. Liu H, Li J, Xu X, et al. Highly graphitic carbon black-supported platinum nanoparticle catalyst and its enhanced electrocatalytic activity for the oxygen reduction reaction in acidic medium. *Electrochim Acta*. 2013;93:25-31.
14. Ercolano G, Farina F, Cavaliere S, Jones DJ, Rozière J. Towards ultrathin Pt films on nanofibres by surface-limited electrodeposition for electrocatalytic applications. *J Mater Chem A*. 2017;5(8):3974-3980.
15. Marichy C, Ercolano G, Caputo G, et al. ALD SnO_2 protective decoration enhances the durability of a Pt based electrocatalyst. *J Mater Chem A*. 2016;4(3):969-975.
16. Jiménez-Morales I, Cavaliere S, Jones D, Rozière J. Strong metal–support interaction improves activity and stability of Pt electrocatalysts on doped metal oxides. *Phys Chem Chem Phys*. 2018;20(13):8765-8772.
17. Dubau L, Maillard F, Chatenet M, et al. Durability of alternative metal oxide supports for application at a proton-exchange membrane fuel cell cathode—comparison of

antimony- and niobium-doped tin oxide. *Energies*. 2020; 13(2):403.
18. Nabil Y, Cavaliere S, Harkness IA, Sharman JDB, Jones DJ, Rozière J. Novel niobium carbide/carbon porous nanotube electrocatalyst supports for proton exchange membrane fuel cell cathodes. *J Power Sources*. 2017;363:20-26.
19. Jiménez-Morales I, Cavaliere S, Dupont M, Jones D, Rozière J. On the stability of antimony doped tin oxide supports in proton exchange membrane fuel cell and water electrolysers. *Sustain Energy Fuels*. 2019;3(6):1526-1535.
20. Bredol M, Szydło A, Radev I, et al. How the colloid chemistry of precursor electrocatalyst dispersions is related to the polymer electrolyte membrane fuel cell performance. *J Power Sources*. 2018;402:5-23.
21. Roh CW, Choi J, Lee H. Hydrophilic-hydrophobic dual catalyst layers for proton exchange membrane fuel cells under low humidity. *Electrochem Commun*. 2018;97:105-109.
22. Yang H, Ko Y, Lee W, Züttel A, Kim W. Nitrogen-doped carbon black supported Pt–M (M = Pd, Fe, Ni) alloy catalysts for oxygen reduction reaction in proton exchange membrane fuel cell. *Mater Today Energy*. 2019;13:374-381.
23. Forouzandeh F, Li X, Banham DW, et al. Improving the corrosion resistance of proton exchange membrane fuel cell carbon supports by pentafluorophenyl surface functionalization. *J Power Sources*. 2018;378:732-741.
24. Fang Z, Lee MS, Kim JY, Kim JH, Fuller TF. The effect of carbon support surface functionalization on PEM fuel cell performance, durability, and ionomer coverage in the catalyst layer. *J Electrochem Soc*. 2020;167(6):064506.
25. Savych I, Bernard d'Arbigny J, Subianto S, Cavaliere S, Jones DJ, Rozière J. On the effect of non-carbon nanostructured supports on the stability of Pt nanoparticles during voltage cycling: a study of TiO_2 nanofibres. *J Power Sources*. 2014;257:147-155.
26. Kaluža L, Larsen MJ, Zdražil M, Gulková D, Odgaard M. Fuel cell platinum catalysts supported on mediate surface area carbon black supports. *Chem Eng Trans*. 2015;43:913-918.
27. Larsen MJ, Jiménez Morales I, Cavaliere S, et al. Development of tailored high-performance and durable electrocatalysts for advanced PEM fuel cells. *Int J Hydrog Energy*. 2017;42(10):7166-7176.
28. Kaluža L, Larsen MJ, Morales IJ, et al. Synthesis of Pt/C fuel cell electrocatalysts: residual content of chloride and activity in oxygen reduction. *Electrocatalysis*. 2016;7(4):269-275.
29. Jawhari T, Roid A, Casado J. Raman spectroscopic characterization of some commercially available carbon black materials. *Carbon*. 1995;33(11):1561-1565.
30. Zajac J, Groszek AJ. Adsorption of C60 fullerene from its toluene solutions on active carbons: application of flow microcalorimetry. *Carbon*. 1997;35(8):1053-1060.
31. Groszek AJ. Graphitic and polar surface sites in carbonaceous solids. *Carbon*. 1987;25(6):717-722.
32. Martens S, Asen L, Ercolano G, et al. A comparison of rotating disc electrode, floating electrode technique and membrane electrode assembly measurements for catalyst testing. *J Power Sources*. 2018;392:274-284.
33. Groszek AJ, Partyka S. Measurements of hydrophobic and hydrophilic surface sites by flow microcalorimetry. *Langmuir*. 1993;9(10):2721-2725.
34. Van Oss CJ, Chaudhury MK, Good RJ. Interfacial Lifshitz–van der Waals and polar interactions in macroscopic systems. *Chem Rev*. 1988;88(6):927-941.
35. Tuinstra F, Koenig JL. Raman spectrum of graphite. *J Chem Phys*. 1970;53(3):1126-1130.
36. Wang Y, Serrano S, Santiago-Avilés J. Raman characterization of carbon nanofibers prepared using electrospinning. *Synth Met*. 2003;138:423-427.
37. Maslova OA, Ammar MR, Guimbretière G, Rouzaud JN, Simon P. Determination of crystallite size in polished graphitized carbon by Raman spectroscopy. *Phys Rev B*. 2012; 86(13):1-5.
38. De Miguel SR, Scelza OA, Román-Martínez MC, Salinas-Martínez De Lecea C, Cazorla-Amorós D, Linares-Solano A. States of Pt in Pt/C catalyst precursors after impregnation, drying and reduction steps. *Appl Catal A*. 1998;170(1):93-103.
39. Torres GC, Jablonski EL, Baronetti GT, et al. Effect of the carbon pre-treatment on the properties and performance for nitrobenzene hydrogenation of Pt/C catalysts. *Appl Catal A*. 1997;161(1-2):213-226.
40. Guerrero-Ruiz A, Badenes P. Rodríguez-Ramos I. Study of some factors affecting the Ru and Pt dispersions over high surface area graphite-supported catalysts. *Appl Catal A*. 1998; 173(2):313-321.
41. Fraga MA, Jordão E, Mendes MJ, Freitas MMA, Faria JL, Figueiredo JL. Properties of carbon-supported platinum catalysts: role of carbon surface sites. *J Catal*. 2002;209(2):355-364.

SUPPORTING INFORMATION

Additional Supporting Information may be found online in the supporting information tab for this article.

How to cite this article: Jiménez-Morales I, Reyes-Carmona A, Dupont M, et al. Correlation between the surface characteristics of carbon supports and their electrochemical stability and performance in fuel cell cathodes. *Carbon Energy*. 2021;1-12. https://doi.org/10.1002/cey2.109